Kirk-Othmer Encyclopedia of Chemical Technology.
Copyright © John Wiley & Sons, Inc. All rights reserved.

SEMICONDUCTORS, AMORPHOUS

1. Introduction

Since 1970 the subject of amorphous semiconductors, in particular silicon, has progressed from obscurity to product commercialization such as active matrix liquid-crystal displays, linear sensor arrays for facsimile machines, inexpensive solar panels, electrophotography, etc. Many other applications are at the developmental stage such as medical imaging, spatial light modulators for optical computing, and optical filters (1,2).

The success has been primarily due to the developments that occurred in the early 1970s (3) at the University of Dundee (United Kingdom) where it was demonstrated that a device-quality amorphous silicon semiconductor (a-Si) could be produced with the following features: low concentration of defects, high photosensitivity, ability to be doped, and no size limitation.

There is another class of amorphous semiconductors based on chalcogens that predate the developments that have occurred in a-Si. Because their use has been limited, eg, to switching types of devices and optical memories, this discussion is restricted to the optoelectronic properties of a-Si-based alloys and their role in some applications.

2. Classification

Amorphous semiconductors are solids in which the atoms retain well-defined local, or nearest neighbor, order, but lack long-range periodic order of crystalline solids, and the local bonding between atoms is characterized predominantly by covalent forces (4,5). These types of semiconductors are normally synthesized as metastable thin solid films and are to be distinguished from glass that is formed by continuous hardening of a cooled liquid. Amorphous material is a solid in internal equilibrium in which there is, just as in crystalline solids, a definite set of equilibrium positions about which the atoms oscillate. However, in contrast to crystalline solids, the amorphous materials do not exhibit translational symmetry, ie, there is no long-range order.

The tetrahedrally bonded materials, such as Si and Ge, possess only positional disorder; however, materials of this type exhibit high density of defect states (DOS). It is only with the addition of elements, such as hydrogen and/or a halogen, typically fluorine, that the DOS is reduced to a point such that electronic device applications emerge. These materials contain up to ~10 atomic % hydrogen, commonly called hydrogenated amorphous silicon (a-Si:H).

3. Effect of Disorder

The short-range order in a material is important in determining optoelectronic properties. For example, X-ray and electron diffraction experiments performed on amorphous silicon (a-Si) and germanium (a-Ge) have

revealed that the nearest neighbor environments are approximately the same as those found in their crystalline counterparts (6); photoemission experiments performed on a-Si show that the DOS in valence and conduction bands are virtually identical to the corresponding crystal with the exception that the singularities (associated with periodicity) present in the latter are smeared out in the former.

Hence, the concept of DOS, $g(E)$, the number of one-electron states in the energy, E, range, $E+dE$, is valid along with the determination of average occupancy using Fermi-Dirac statistics. Another valid concept is mobility, μ (velocity per unit applied electric field), which depends on the entire state of the system. For a perfectly periodic crystal at absolute zero ($T = 0$ K), all the states are delocalized and the value of μ is infinite. In amorphous semiconductors, intense scattering, due to large fluctuations in the one-electron potential, can greatly reduce the value of μ. Once $g(E)$ and $\mu(E)$ are known, the optoelectronic properties of the material can be determined.

As is to be expected, inherent disorder has an effect on electronic and optical properties of amorphous semiconductors providing for distinct differences between them and the crystalline semiconductors. The inherent disorder provides for localized as well as nonlocalized states within the same band such that a critical energy, E_c, can be defined by distinguishing the two types of states (4). At $E = E_c$, the mean free path of the electron is on the order of the interatomic distance and the wave function fluctuates randomly such that the quantum number, k, is no longer valid. For $E < E_c$, the wave functions are localized and for $E > E_c$, they are nonlocalized. For $E > E_c$, the motion of the electron is diffusive and the extended state mobility is $\sim$10 cm^2/sV. For $E < E_c$, conduction takes place by hopping from one localized site to the next. Hence, at $E = E_c$, μ goes through a transition with a variation of $\sim 10^3$. This leads to the concept of the mobility edge at $E = E_c$ and correspondingly at the valence band edge, $E = E_v$; $E_c - E_v$ is defined as the μ-gap that leads to the existence of semiconducting behavior in amorphous materials.

4. Growth of Amorphous Silicon

By far, the most widely studied (7) and used deposition technique for preparing amorphous silicon is the plasma-enhanced chemical vapor deposition (PECVD) technique, which typically utilizes a capacitively coupled multichamber system, as shown in Fig. 1. A gas, such as SiH_4, is allowed to pass at a controlled rate between the two plates and the plasma is generated using direct current (dc), audio, radio frequency (rf), or microwave frequencies. A variety of species are produced, such as atoms, free radicals, and stable and unstable ions. The mean energy of the electron is on the order of a few electron volts and electron temperature can be up to 100 times higher than that of the gas. Hence, the electrons possess enough energy to break down the molecular bonds.

The defect state density within the μ-gap or the DOS is critically controlled by the deposition temperature, T_s, of the substrates; the DOS decreases by several orders of magnitude when T_s is raised from 300 to 570 K (8). This change in DOS has been attributed to basic structural change from a polymeric-type (SiH_n) structure, for samples deposited at low temperature, to a monohydride (SiH) structure for higher T_s samples (9). The pressure of the gases during deposition also affects the properties of the film because gas-phase polymerization is encouraged at high pressures with the consequence that $SiH_2$and SiH_3 grouping within the film becomes more pronounced and again DOS increases in the film.

The relative abundance of neutral SiH_4 and H_2 species have been measured as a function of power, pressure, flow rate, and dilution. For low power levels, eg, 5 W, up to 50% of the SiH_4 gas is dissociated and the percentage increases to 80% for a power of 50 W. The decomposition of SiH_4 gas proceeds more readily with lower flow rates. These observations, coupled with infrared (ir) measurements performed on the films, suggest that deposition under conditions in which the silane gas is not entirely decomposed leads to a majority of SiH units, whereas those deposited under conditions in which silane is strongly dissociated contain a majority of dihydride units leading to a deterioration of the semiconductor. Also, when the dwell time of SiH_4 in the plasma

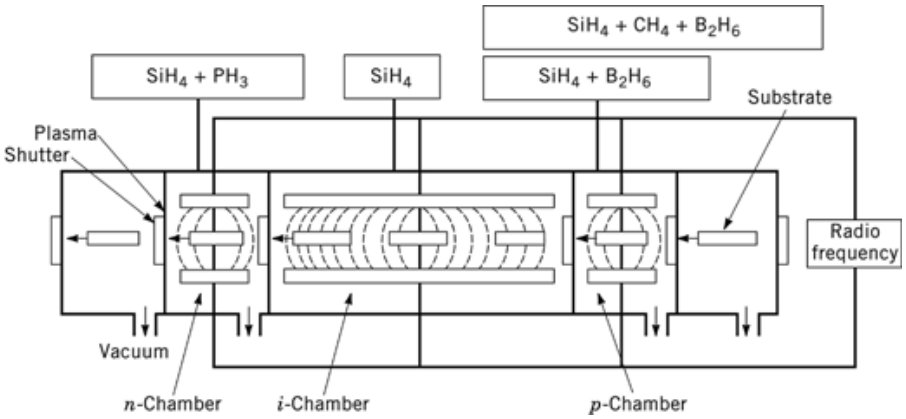

Fig. 1. Multichamber PECVD reaction chamber apparatus for fabrication of *a*-Si:H films, where the *i*-chamber represents the deposition of the intrinsic layer; *n*-chamber, the deposition of *n*-type layer; and *p*-chamber, the deposition of *p*-type layer.

Table 1. Electron Impact Dissociative Processes Operative in Silane Plasma[a]

Dissociation process	Enthalpy of reaction ΔH, eV
$e^- + SiH_4 \rightarrow SiH_2 + H_2 + e^-$	2.2
$e^- + SiH_4 \rightarrow SiH_3 + H + e^-$	4.0
$e^- + SiH_4 \rightarrow Si + 2\ H_2 + e^-$	4.2
$e^- + SiH_4 \rightarrow SiH + H_2 + H + e^-$	5.7
$e^- + SiH_4 \rightarrow SiH^+_2 + H_2 + 2e^-$	11.9
$e^- + SiH_4 \rightarrow SiH^+_3 + H + 2\ e^-$	12.3
$e^- + SiH_4 \rightarrow SiH^* + H_2 + H + e^-$	8.7

[a]Quantities ΔH are enthalpies of formation of the species; the densitiese of SiH_2 and SiH_3 species in the plasma have been shown to be larger than other species.

region increases, the resultant film exhibits a pronounced peak at 2090 cm^{-1} from the ir spectra corresponding to SiH_2 inclusion.

Various plasma diagnostic techniques have been used to study the SiH_4 discharges and results have helped in the understanding of the growth kinetics. These processes can be categorized as rf discharge electron kinetics, plasma chemistry including transport, and surface deposition kinetics.

The primary process of SiH_4 decomposition is electron impact that produces a large number of different neutral and ionic species as shown in Table 1. The density of SiH_2 and SiH_3 neutral species produced has been found to be much larger than the density of the ions. For example, mass spectrometric data for silane discharges indicate that the density of ionic species is lower by $\sim 10^4$ compared with the density of neutral species. Further, mass spectrometer signals of ionic species, such as SiH^+_3, SiH^+_2, SiH^+, SiH^+, and $Si_2H^+_5$, increase by more than two orders of magnitude as the rf power is increased, eg, from 2 to 20 W. A rapid rise in the population of ions, with power, implicitly means an increase in electron density.

Table 2 shows the predominant reactions that take place during the transport of the species produced by electron impact dissociation to the substrate. The large rate of the insertion reaction of SiH_2 with SiH_4 results in the production of Si_2H_6 and is one of the mechanisms by which the powders observed using silane decomposition can be formed. The growth mechanism is complex because virtually all types of species reach the substrate surface. There is considerable evidence that the precursor for growth is primarily SiH_3.

Table 2. Reactions Within Plasma During Transport of Species Produced by Electron Impact Dissociation of Silane

Reaction	Enthalpy of reaction DH, eV
$SiH_4+H \rightarrow SiH_3+H_2$	−0.5
$SiH_2+SiH_4 \rightarrow Si_2H_6$	−2.1
$SiH_2+H_2 \rightarrow SiH_4$	−2.2
$SiH_3+SiH_3 \rightarrow Si_2H_6$	−3.2
$Si_2H_6 \rightarrow SiH_2+SiH_4$	2.1
$SiH^+_2+SiH_4 \rightarrow SiH_3+SiH^+_3$	−0.04
$SiH^+_3+SiH_4 \rightarrow Si_2H^+_5+H_2$	−0.12

The state-of-the-art a-Si:H films (Table 3) are deposited at the rate of 1–3 A/s with the gas utilization rate on the order of 15%. Larger gas utilization rates, hence larger deposition rates, usually result in inferior properties than those indicated in Table 3. Increasing the deposition rate by merely increasing the power leads to dust formation. The use of higher excitation frequency can lead to deposition rates in excess of 15 A/s and still give relatively good film properties (7).

5. Properties

As discussed, an inclusion of an element, such as H, plays a crucial role in determining the properties of the a-Si:H material. This can be illustrated by considering the results of sputtered Si prepared in a reactive H environment. Figure 2 shows the effect of H on the electronic properties of a-Si with all the samples prepared at 200°C. In Fig. 2 the dark conductivity, σ_D, is plotted as a function of $10^3/T$ with hydrogen pressure. The hydrogen content of the films increases from curves A to F. With the addition of 20 atomic % H to the films, curve F, an activated behavior over several orders of magnitude in the conductivity, results that corresponds to extended state conduction above E_c. This change in the conduction behavior is due to the reduced DOS within the μ-gap.

The optoelectronic properties of the a-Si:H films depend on many deposition parameters, such as the pressure of the gas, flow rate, substrate temperature, power dissipation in the plasma, excitation frequency, anode–cathode distance, gas composition, and electrode configuration. Deposition conditions that are generally employed to produce device-quality hydrogenated amorphous Si (a-SiH) are as follows: gas composition = 100% SiH_4or diluted in H_2; flow rate is high, ∼40 sccm; pressure is low, 26–80 Pa (200–600 mtorr); deposition temperature = 250°C; rf power is low, <25 mW/cm^2; and the anode–cathode distance is ∼1–4cm.

Table 3 summarizes some of the present state-of-the-art parameters obtained for undoped and doped a-SiH(F) material thus produced. The device-quality material exhibits semiconductivity because ln σ_D versus $10^3/T$ exhibits a straight line with a conductivity activation energy of ∼0.85 eV, which is approximately equal to half the band gap of ∼1.75 eV. Typically the dark conductivity $<10^{-10}(\Omega\cdot\text{cm})^{-1}$ changes to $>10^{-5}(\Omega\cdot\text{cm})^{-1}$ under light illumination (Global AM1.5 sun illumination of intensity 100 mW/cm^2). The DOS (or defect) is found to be low with a dangling bond (DB) density, as measured by electron spin resonance (esr) of $\sim 10^{15}$ cm^{-3}. The inherent disorder possessed by these materials manifests itself as band tails that emanate from the conduction and valence bands and are characterized by exponential tails with an energy of 25 and 45 meV, respectively; the broader tail from the valence band provides for dispersive transport (shallow defect controlled) for holes with a low drift mobility of 10^{-2}cm^2/(s ·V), whereas electrons exhibit nondispersive transport behavior with a higher mobility of ∼1 cm^2/(s· V). Hence, the material exhibits poor minority (hole) carrier transport with a diffusion length <0.5 μm, which puts a design limitation on electronic devices, such as solar cells.

Table 3. Typical Optoelectronic Parameters Obtained for *a*-Si:H(F) Alloys

Parameter	Value
Undoped	
hydrogen content, C_H, %	~10
dark conductivity at 300 K, σ_D, $(\Omega\cdot cm)^{-1}$	$\sim 10^{-10}$
activation energy, ΔE or E_s, eV	~0.8–0.9
pre-exponent conductivity factor, σ_o, $(\Omega\cdot cm)^{-1}$	$>10^3$
optical band gap at 300 K, E_g, eV	1.7–1.8
E_g variation with temperature, $E_g(T)$, eV/K	$2–4 \times 10^{-4}$
density of states	
at minimum, g_{min} or $g(E_f)$, $cm^{-3}\ eV^{-1}$	$>10^{15}–10^{17}$
at conduction band edge, $g(E_c)$, $cm^{-3}\ eV^{-1}$	$\sim 10^{21}$
electron spin resonance spin density, N_s, cm^{-3}	$\sim 10^{15}$
infrared spectra, cm^{-1}	2000/640
photoluminescence peak at 77 K, eV	~1.25
extended state mobility	
electrons, μ_n or μ_e, $cm^2/(s\cdot eV)$	>10
holes, μ_p or μ_h, $cm^2/(s\cdot eV)$	~1
drift mobility	
electrons, μ_n or μ_e, $cm^2/(s\cdot eV)$	~1
holes, μ_p or μ_h, $cm^2/(s\cdot eV)$	$\sim 10^{-2}$
tail slope, meV	
conduction band	25
valence band	40
hole diffusion length, μm	~<0.5
Doped amorphous	
n-type ~1 addition PH_3 to gas phase	
σ_d, $(\Omega\cdot cm)^{-1}$	$\sim 10^{-2}$
ΔE, eV	~0.2
p-type ~1% addition B_2H_4 to gas phase	
σ_d $(\Omega\cdot cm)^{-1}$	$\sim 10^{-3}$
ΔE, eV	~0.3
Doped microcrystalline	
n-type ~1% PH added to dilute SiH_4:H_2[a] gas mixture	
σ_d, $(\Omega\cdot cm)^{-1}$	≥1
ΔE, eV	≤0.05
p-type ~1% B_2H_6 added to dilute SiH_4:H_2 gas mixtures	
σ_d, $(\Omega\cdot cm)^{-1}$	≥1
ΔE, eV	≤0.05

[a]Or 500 vppm PH_3 added to SiF_4:H_2 (8:1) gas mixture. Relatively high power is involved.

The low DOS achieved in *a*-Si:H enables it to be readily doped, a prerequisite for any device application; *n*- and *p*-type doping is achieved by the addition of PH_3 and B_2H_6 to SiH_4 in the gas phase, respectively. Figure 3, a plot of σ_D and conductivity activation energy, ΔE, as a function of PH_3 and B_2H_6 content, shows that the most heavily *n*-type doping results in $\sigma_D \sim 10^{-2} (\Omega\cdot cm)^{-1}$. By manipulating the plasma (using SiF_4 and H_2) or heavily diluting SiH_4 plasma with H_2, micro- (or nano)crystalline *n*- and *p*-materials can be made with conductivities in excess of $1(\Omega\cdot cm)^{-1}$.

Another parameter of relevance to some device applications is the absorption characteristics of the films. Because the *k* quantum is no longer valid for amorphous semiconductors, *a*-Si:H exhibits a direct band gap

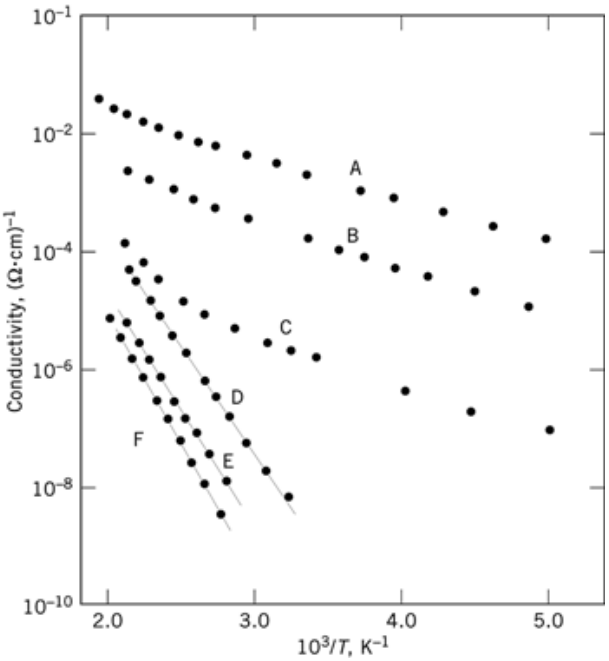

Fig. 2. Dark conductivity, σ_D, versus $10^3/T$ for sputtered a-Si:H samples prepared at T_s of 200°C using partial hydrogen pressure between 0 and 0.13 Pa (0–1 mtorr). Hydrogen content (atomic %) and hydrogen partial pressure are as follows for each curve: A, 0 atomic (at) %; B, 1 at%, 0.002 Pa; C, 2 at%, 0.0067 Pa; D, 10 at%, 0.02 Pa; E, 15 at%, 0.05 Pa; and F, 20 at%, 0.133 Pa. To convert Pa to mtorr, multiply by 7.5.

(∼1.70 eV) in contrast to the indirect band gap nature in crystalline Si. Therefore, a-Si:H possesses a high absorption coefficient such that to fully absorb the visible portion of the sun's spectrum only 1 μm is required in comparison with >100 μm for crystalline Si. Further improvements in the material are expected to result from a better understanding of the relationship between the processing conditions and the specific chemical reactions taking place in the plasma and at the surfaces that promote film growth.

6. Applications of *a*-Si-Based Semiconductors

As discussed previously, inherent disorder possessed by a-Si:H alloy limits the mobility of the free carriers (electrons and holes) to ∼ 10 $cm^2/(s\cdot V)$; this is compared with crystalline Si, in which the electron mobility is 1500 $cm^2/(s\cdot V)$. However, crystalline Si is expensive to manufacture and its size is limited to about 30 cm in diameter. Many applications discussed have either emerged or been identified which preclude the use of crystalline Si because of cost, size, or both. The basic commonality in these applications is the ability to fabricate devices on areas much larger than can be addressed by crystalline Si. Furthermore, these applications are not demanding in terms of speed, which then provides a-Si:H alloy with a distinct competitive advantage.

Figure 4 shows the basic construction of the devices used in different applications, involving the deposition of multilayers of a-Si:H of intrinsic (i), doped (n^+,p^+), and closely allied films, such as amorphous silicon nitride, SiN, and transparent conducting oxide (TCO). As in crystalline semiconductors, the basic building block is a junction (p–n) or thin-film transistor. Attempts to fabricate p–n junctions (using a-Si:H) have thus far exhibited insignificant rectification, as shown in Fig. 5. The reason is that during the process of doping with B or P, extra

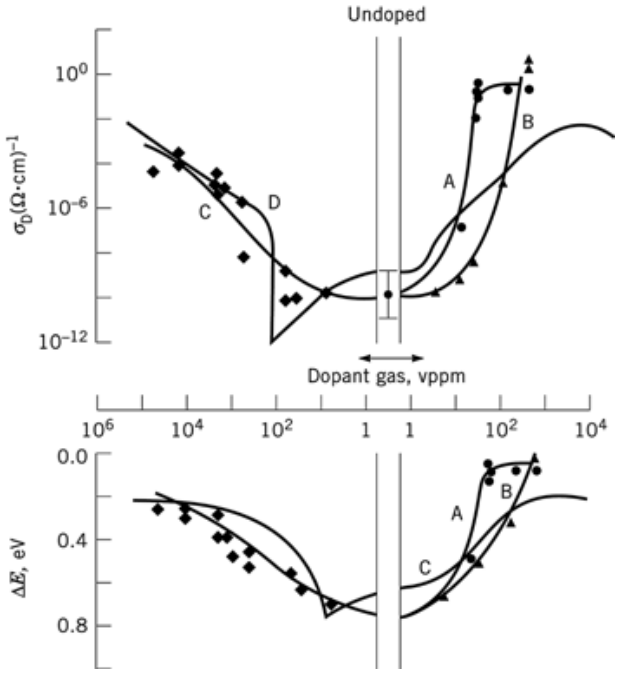

Fig. 3. The room temperature dark conductivity, σ_D $(\Omega\cdot cm)^{-1}$, and conductivity activation energy, ΔE in eV, plotted as A, a function of vppm of AsH_3 (•); B, PH_3 (▲); and C, B_2H_6 (ϒ) into the premix gas ratio of SiF_4:$H_2 = 10$:1. The p to n transition (left to right) refers to a-Si:F:H alloy, and D refers to doping characteristics for this alloy.

defect states are introduced within the gap, which leads to an increase in the generation–recombination current, thus precluding viable rectification. Instead of this type of junction, an i-layer is inserted between the p^+ and n^+ layers with the charge separation occurring within the intrinsic layer; a basic requirement being that the p^+ and n^+ layers should be thick enough to sustain a depletion width. Figure 5 also shows the forward and reverse bias characteristics of a p–i–n junction with a much improved rectification ratio $> 10^5$ at 0.8 V. The other type of structure is a field-effect transistor (FET) or thin-film transistor (TFT) and a typical construction is shown in Fig. 4. In this case, the conductivity of the semiconducting layer is altered by the application of an external voltage applied to the gate metal electrode. For example, an application of a positive gate voltage leads to a negative charge induced into the a-Si:H layer. The consequence is that the bands (valence and conduction) bend downward (accumulation layer) and conductivity (the current monitored between source and drain contacts) rises. An example of this is given in Fig. 6, where it can be seen that with gate voltage of only a few volts, the source–drain current is altered by a factor of 10^6. These devices are used in some important areas, eg, solar cells, fax machines, and active matrix liquid- crystal displays.

The fact that excellent rectification can be demonstrated with these p–i–n junctions, together with high photosensitivity and the ability to deposit over large areas, leads to natural usage as a solar cell (see). The three primary parameters of a solar cell are the open-circuit voltage (V_{oc}), the short-circuit current (J_{sc}), and the fill factor (FF) with a theoretical maximum of 1.1 V, 22 mA/cm^2, and 0.8, respectively, which leads to a conversion efficiency, η, of ∼19%. The solar cell is generally constructed on a transparent conducting oxide, SnO_2 (see Fig. 4). A thin (10 nm) a-Si:C:B:H (p^+ material) is deposited; in this, C is added to the p^+ material during growth to widen the band gap and thus allow light to enter more effectively into the junction region primarily located at the p-i interface. After the p^+-layer deposition, an i-layer of thickness between 300 and

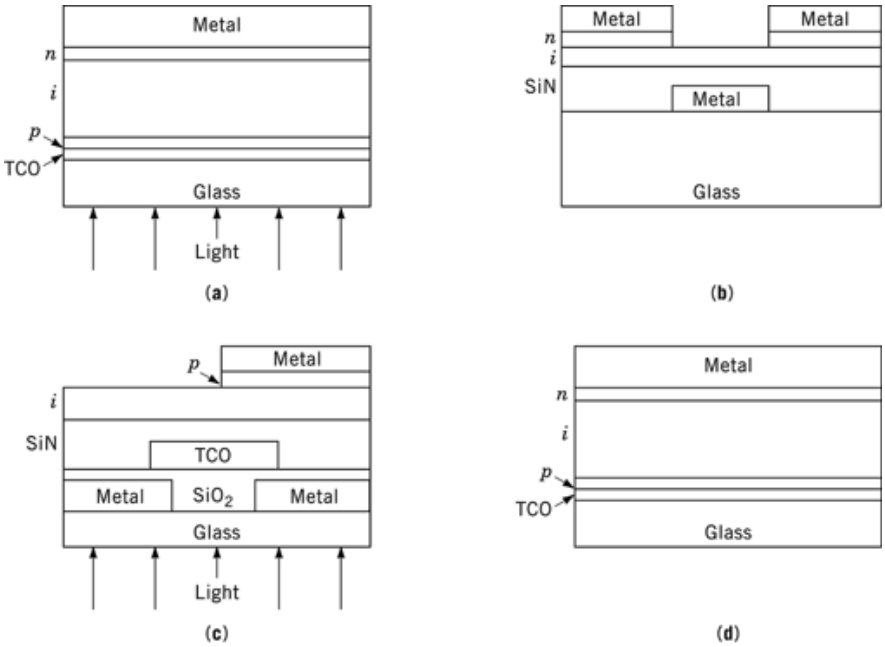

Fig. 4. Some electronic device applications using amorphous silicon: (**a**) solar cell, (**b**) thin-film transistor, (**c**) image sensor, and (**d**) nuclear particle detector. TCO = transparent conducting oxide.

700 nm is deposited, followed by an n^+-layer (∼20 nm) deposition, and the structure completed with a highly reflective contact, such as Ag. In order to minimize the losses, this structure is manipulated further with the insertion of extra layers, such as a graded layer between the p^+- and *i*-layer to minimize recombination losses that could exist at that discontinuity. Silver is often replaced with a two-layer reflective structure such as zinc oxide/Ag. Generally, textured SnO_2 is used to promote multiple internal reflections to enhance the current produced by the device. Using some of these techniques, the efficiency of a single *p–i–n* junction in excess of 11% has been obtained. To further enhance the performance a concept of tandem junctions(or multijunction device) is employed. In this approach, the low energy photons are directed to solar cells made from smaller band gap material (eg, *a*-Si:Ge:H) and the high energy photons are directed to wide band gap cells where their energy is not dissipated by creating electron–hole pairs with energies much in excess of the band gap. The cells, whose active semiconductors possess different band gaps, are connected in series and stacked on top of each other with the widest band gap material facing the incident illumination. The low energy photons pass through the cells until they reach a band gap semiconductor that can utilize them. The thickness and values of the band gaps are arranged such that the current generated from the constituent cells are the same. Calculations leading to the design of multijunction stack arrays have been performed, indicating a maximum conversion efficiency of ∼24% with stacks consisting of 1.45, 1.7, and 2.0 eV band gap materials. Experimentally, $\eta > 15\%$ has been achieved for a three-stacked cell on a stainless steel substrate, and $\eta > 10\%$ for large area modules on a glass substrate that exhibit <15% degradation over several hundred hours of constant testing (7).

The *p–i–n* junctions of virtually similar construction are also used as contact linear array image sensors in facsimile machines. An advantage is that they eliminate the need for magnification lenses that are used in conjunction with charge coupled device (CCD) sensors, constructed from crystalline Si devices. In a facsimile machine, the sensor unit consists of an illuminator, a compact optical guide, and a long photosensor array connected to the scanner. Light from the light-emitting diode (LED) arrays illuminates the document and the

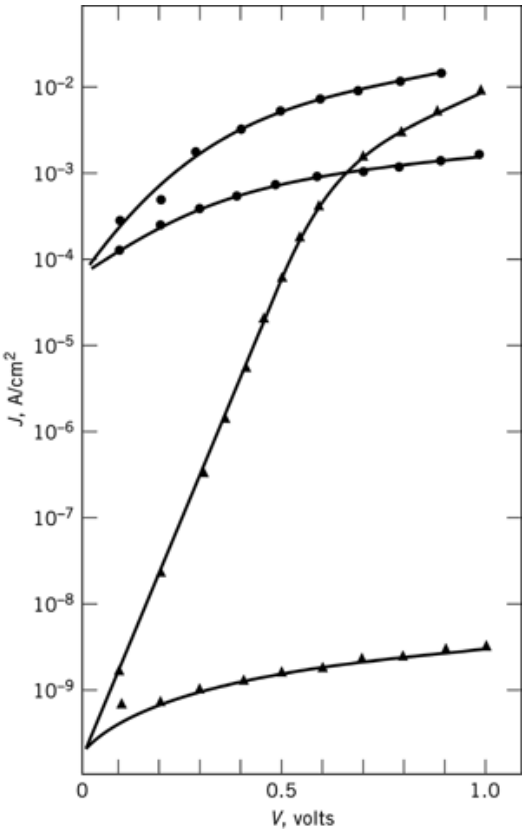

Fig. 5. Dark J–V (current–voltage) characteristics of p–n (•) and p–i–n (▲) junctions at 295 K.

reflected signal is guided by the rod lens array onto the a-Si:H p–i–n junction photosensor array (see Fig. 4). The p–i–n junctions are constructed in a pixelized fashion with the number dictated by the resolution requirements, eg, 200 dots/in. (80 dots/cm) necessitates an excess of 1800 pixels for a page width array. The junctions are operated in reverse bias, with typical off-current of $\sim 10^{-13}$ amps, and under illumination the current rises by several orders of magnitude to excess of 10^{-9}amps. The photocurrent generated is proportional to the light intensity reaching the pixels. By operating the devices in the charge collection mode and with use of appropriate circuitry, the output of the device is proportional to light intensity. The elements are attached to read-out integrated circuits which then transmit the data to the receiver.

In an active matrix liquid crystal (LC) display application, a single TFT for each picture element (pixel) is incorporated, as shown in Fig. 7. In a display of 12 in. ($\sim$30 cm) diagonal size, pixels in excess of 10^6 have been incorporated. The display consists of two plates between which the LC is sandwiched and backlit. The LC possesses the property that when its twist is altered, the transmission characteristics are changed. $S_1 \ldots S_n$ and $G_1 \ldots G_n$ are bus lines for the source and gate electrodes, and the drain, D, contact is connected to each TCO square (see Fig. 7). The LC is in series with the drain circuit and behaves electrically as a capacitor, C_{LC}. The addressing scheme involves writing one line at a time, corresponding to a television line, in 63.5 μs. In this time scale, gate G_1 is simultaneously applied to the source lines, ie, zero potential for pixels that are to be turned on. After 63.5 μs, the TFTs that have been addressed (G_1) are turned off and the charge is retained in C_{LC}. In the next 63.5 μs, video data are entered into G_2, and the information for that is simultaneously applied

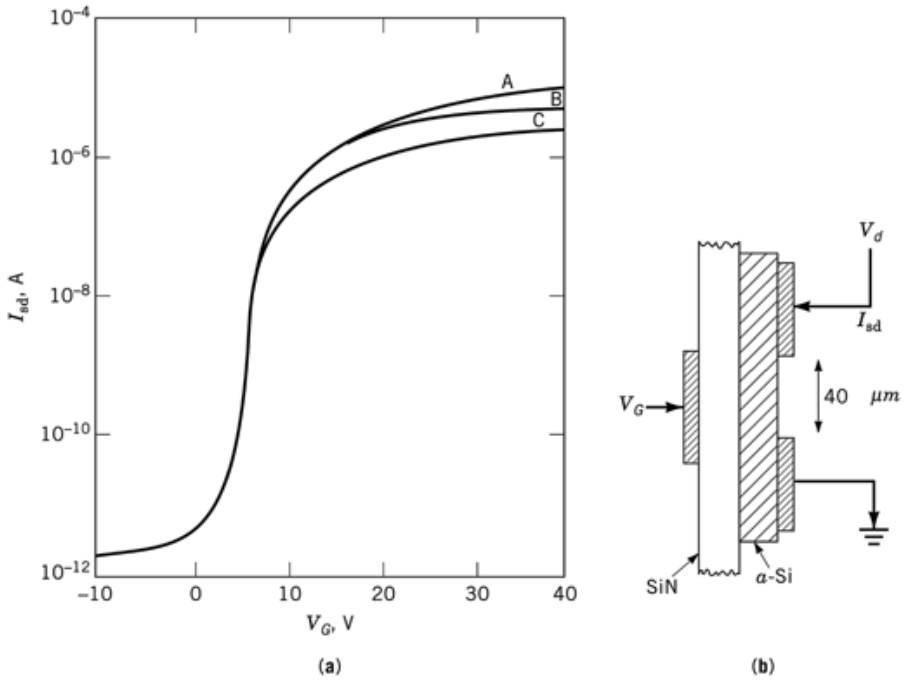

Fig. 6. (**a**) Transfer characteristics of (**b**) a-Si TFT element. The drain current, I_{sd}, is plotted against the gate voltage, V_G, for three drain potentials: A, $V_{d\,=}$ 20V; B, 10 V and C, 2 V.

to the source lines. When all gate buses have been addressed, the scan returns to the first bus line and the process is repeated.

7. Stability of Amorphous Silicon

Stability is one of the principal issues confronting the eventual commercialization of solar cells for large-scale power applications. There has been an increasing amount of data showing that good stability can be attained in a-Si alloy devices. In a solar cell device configuration, the degradation is seen primarily as a decrease in the fill factor and J_{sc}, but the device can be restored to its original performance level upon annealing at 175°C for 30 min. The amount of degradation is a function of the operating conditions: it is greatest at V_{oc}, reduces at J_{sc}, and is virtually eliminated under far reverse bias conditions. These observations have been associated with the so-called Staebler-Wronski effect (SW), where the application of light can significantly degrade the electronic properties of the material. Two types of states can be distinguished: a fully annealed state attained by slowly cooling the material from ∼500 K to room temperature in the dark (state A); and a light-soaked state attained after application of $\sim 10^{21}$ photons/cm^2 to the material (state B).

There have been many investigations of photoinduced effects in a-Si:H films linked to material parameters. Changes have been observed in the carrier diffusion length, unpaired spin density, density of states in the gap, and ir transmission. The transition from state A to B seems to be induced by any process that creates free carriers, including X-ray radiation and injection (double) from the electrodes. Because degradation in a solar cell is accentuated at the open-circuit voltage conditions, the A to B transition occurs upon recombination of excess free carriers in which the energy involved is less than the band gap. It has been pointed out that this

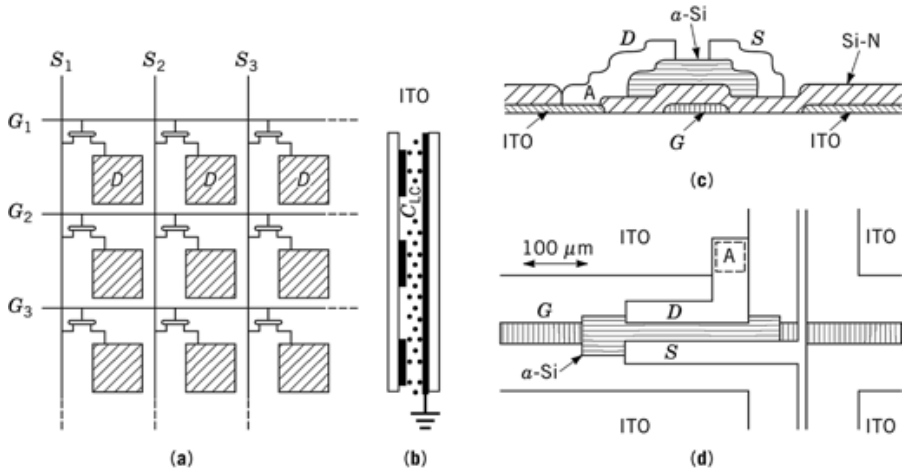

Fig. 7. Schematic layout of addressable liquid crystal (LC) panel: (**a**) plane view, (**b**) side view, (**c**) section through transistor element, and (**d**) TFT in part of matrix array. ITO = indium tin oxide.

transition is a relatively inefficient one and the increase in spin density takes place at a rate of 10^{-8} spins per absorbed photon.

The recovery from state B to A seems to be complete upon annealing, suggesting that state B is metastable and that the photoinduced defects are distinct from the defects present in state A. Various explanations for the SW effect have been put forth but no clear consensus has yet emerged. This degradation remains the major impediment for large- scale usage of amorphous silicon solar cells. The degradation under light illumination is strongly dependant on the thickness of the device used and can be circumvented to a certain extant by the use of multijunction (MJ) devices at the expense of complexity in fabrication. As discussed above, there are several thin cells stacked on top of each other with differing band gaps to absorb a wider portion of the solar spectra (such as *a*-SiH/*a*-SiGeH/*a*-SiGeH). Since they are constructed in a two terminal (2-T) device structure, the band gap and thickness of the active layers are adjusted to yield the same current from each constituent cell. This structure necessitates the use of relatively thick *a*-Si:H junctions (∼2500 A), and hence the device exhibits degradation of (∼20%) within the first 1000 h, with primary degradation occurring in <100 h (10). It should be noted that in the fabrication of the narrow band gap material, such as *a*-SiGe:H, GeH_4 gas is required that is prohibitively expensive. Further as the gas utilization is normally < 10%, the cost goals are difficult to meet. Hence, the use of 2-T tandem solar cell with a micro- (or nano) crystalline Si (nc-Si:H) i-layer in the bottom cell and an *a*-Si:H i-layer in the top cell shows a promising technique in terms of providing an increased spectral response over a wide spectral wavelength range. Such solar cells (termed as "micromorph" solar cells) can produce an initial AM1.5 conversion efficiency of ∼13% in small area and ∼12% in large area modules (11). However, these micromorph solar cells also contain a relatively thick (∼4000A) *a*-Si:H layers junction (top cell) due to the current matching constraint from the bottom *nc*-SiH device. As a result, majority of the power (∼70%) results from the unstable thick *a*-Si:H portion. This structure also experiences a significant degradation under light illumination. To circumvent the instability problems in a 2-T MJ device structure, another proposal is the use of a much simpler 4 terminal (4-T) thin-film silicon based MJ solar cell configuration, in which the current matching constraint is released from each constituent cell. For example, two cells (*a*-Si:H and stable low band gap *nc*-Si:H cells) are separated via an insulating material (eg, glass or SiN) and stable device effeciency of >9% has been demonstrated with a potentail to exceed 16% with further development (12).

8. Economic Aspects

Industry based on the use of amorphous silicon represents a multibillion dollar market and is growing at a rapid rate. Major sales are in the display area with numerous companies, eg, Toshiba, Sharp, and AU Optronics involved; in the electrophotography arena, the companies that dominate are Canon, Minolta, and Sharp. Although solar energy attracts the most attention, it is in fact quite a small revenue earner for the *a*-Si-based industry, as it commands ∼5% of the annual market of >1000 MW/year with an average sale price of $3/watt, the primary companies producing these products are Sanyo (Japan), Kaneka (Japan), ECD (USA). Nevertheless, the use of solar panels is expanding at rate of 20–30%/year and the consensus is that thin-film silicon could make a major contribution toward energy production, using photovoltaics, as this is likely to be the cost-effective solution to energy needs.

BIBLIOGRAPHY

"Semiconductors (Amorphous)" in *ECT* 3rd ed., Vol. 20, pp. 654-673, by D. Adler, Massachusetts Institute of Technology; in *ECT* 4th ed., Vol. 21, pp. 750–763, by A. Madan, MVSystems, Inc.; "Semiconductors Amorphous" in *ECT* (online), posting date: December 4, 2000, by A. Madan, MVSystems, Inc.

Cited Publications

1. R. Biswas, G. Ganguly, E. Schiff, R. Carius, M. Kondo, eds., *MRS Proc.* **808** (2004).
2. A. Madan and M. Shaw, *The Physics and Applications of Amorphous Semiconductors*, Academic, San Diego, Calif., 1988.
3. W. E. Spear and P. G. LeComber, *J. Noncryst Solids* **727**, 8 (1972); A. Madan, Ph.D dissertation, University of Dundee, U.K., 1973; W. E. Spear and P. G. LeComeber, *Phil. Mag.* **33**, 935 (1976).
4. N. F. Mott and E. A. Davis, *Electronic Transport in Non-Crystalline Materials*, Clarendon Press, Oxford, U.K., 1979.
5. R. Zallen, *Physics of Amorphous Solids*, Wiley, New York, 1983.
6. S. C. Moss and J. F. Gracyzk, *Phys. Rev. Lett.* **23**, 1167 (1969).
7. G. Bruno, P. Capezzuto, and A. Madan, eds., *Plasma Deposition of Amorphous Silicon Based Materials*, Academic, New York, 1995.
8. A. Madan, P. G. LeComber, and W. E. Spear, *J. Noncryst. Solids* **20**, 239 (1976).
9. G. Lucovsky, R. Nemanich, and J. Knights, *Phys. Rev.* **B19**, 2064 (1979).
10. J. Yang and S. Guha, *Appl. Phys. Lett.* **70**, 2975 (1997).
11. K. Yamamoto and co-workers, IEEE PV Conference, p. 1428, 2000.
12. A. Madan, *MRS Proc.* **814**, 12.9 (2004).

ARUN MADAN
MVSystems, Inc.

Related Articles

; ;